Inorganic Chemistry

Article

pubs.acs.org/IC

Protein-Mediated Synthesis of Nanosized Mn-Doped ZnS: A Multifunctional, UV-Durable Bio-Nanocomposite

Abhinandan Makhal,[†] Soumik Sarkar,[†] and Samir Kumar Pal*

Department of Chemical, Biological and Macromolecular Sciences, S. N. Bose National Centre for Basic Sciences, Block JD, Sector III, Salt Lake, Kolkata 700 098, India

Supporting Information

ABSTRACT: The design of synthetic nanoparticles (NPs) capable of recognizing given chemical entities in a specific and predictable manner is of great fundamental and practical importance. Herein, we report a simple, fast, water-soluble, and green phosphine free colloidal synthesis route for the preparation of multifunctional enzyme-capped ZnS bionanocomposites (BNCs) with/without transitional metal-ion doping. The enzymes α-Chymotrypsin (CHT), associated with the NPs, are demonstrated as an effectual host for organic dye Methylene Blue (MB) revealing the molecular recognition of such dye molecules by the BNCs. An effective hosting of MB in the close proximity of ZnS NPs (with ~3 nm size) leads to photocatalysis of the dyes which has further been investigated with doped-semiconductors. The NP-associated enzyme α-CHT is found to be active toward a substrate (Ala-Ala-Phe-7-amido-4-methyl-coumarin), hence leads to significant enzyme catalysis. Irradiation induced luminescence enhancement (IILE) measurements on the BNCs clearly interpret the role of surface capping agents which protect against deep UV damaging of ZnS NPs.

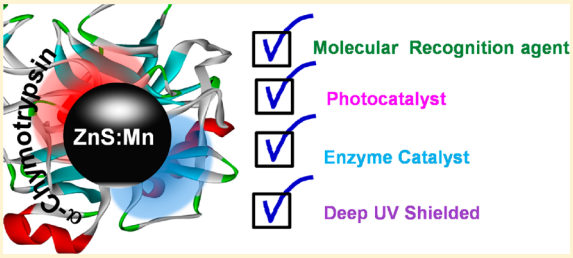

1. INTRODUCTION

The critical role that dopants play in semiconductor structure has stimulated research on the properties and the potential applications of doped semiconductor nanoparticles (NPs).[1,2] The control of optoelectronic properties of such semiconductor NPs using different doping is found to be quite efficient,[3] such as, large magneto-optical effect,[4,5] efficient sensitized impurity luminescence,[4,6−8] and quantum size effects on impurity-carrier binding energies.[9] Manganese (Mn)-doped zinc chalcogenide NPs have been explored as alternatives to popularly used CdSe QDs with advantages of lower toxicity and larger Stokes shift.[10] The synthesis of such Mn-doped zinc sulphide (ZnS) NPs (diameter <5 nm) by the solvothermal method[11] has already been reported. However, the synthesis of high-quality Mn-doped ZnS NPs (diameter <5 nm) characterized by a sharp exciton absorption peak and uniform diameter is still a great challenge. In an earlier study[12] various levels in the Mn-doped ZnS nanocluster with relatively smaller diameter (1.2 nm) in reverse micellar environments leading to different relaxation dynamics have been reported. Tunability of the electronic energy depending on the diameter of high-quality Mn-dopped ZnS nanorod has also been evident in recent literature.[10]

The use of proteins and peptides to direct the in vitro syntheses of inorganic materials is attractive for a number of reasons.[13] First, peptides and proteins make bioenabled syntheses of inorganic materials inherently "green" processing which is facilitated at or near room temperature, in aqueous solutions. Second, proteins and peptides can exquisitely control the size, shape, optical properties, and crystal structure of the inorganic product. The major benefit of using peptides and proteins is to produce materials with highly specific or multiple functions; such proteins and peptides may direct the arrangement of enzymatically active composites or produce materials that specifically recognize substrates. To be a suitable biolabeling agents, NPs should have high luminescence efficiency, biocompatibility, and proper surface groups for coupling with biomolecules. To date, however, the obtained doped nanocrystals barely meet these requirements. The consequence of using capping agents on the electronic and defect states of Mn-doped ZnS NPs, which leads to a large enhancement of photoluminescence (PL) intensity of the nanomaterials, has been reported.[14,15] However, a detailed study on the photoselective excited state dynamics and electron migration in such NPs in a biological macromolecular environment is sparse in literature and is one of the motives of the present work. The studies are important in the context that the interaction of NPs with proteins[16] has emerged as a key parameter in nanomedicine and nanotoxicology.[17]

Here we have followed a simple, faster and "green" phosphine free colloidal chemical route[18] for the synthesis of enzyme-capped high-quality Mn-doped ZnS bionanocomposites (BNCs). The enzyme α-Chymotrypsin (CHT)-capped multifunctional BNCs, with average diameter less than 5 nm, are found to be extremely soluble and stable in aqueous solution for several weeks. To investigate the specific role of enzyme environments on the nanomaterial surface, we have also synthesized Cysteine (Cys, sulfur containing amino group)-capped ZnS NPs with less than 5 nm diameter, as a control sample. While steady-state absorption

Received: May 24, 2012
Published: September 19, 2012

   dx.doi.org/10.1021/ic301083g | *Inorg. Chem.* 2012, 51, 10203−10210

and emission spectroscopy explore various electronic states of the Cys/CHT-capped BNCs, picosecond-resolved emission using various excitation/detection wavelengths reveals the relaxation of electrons from specific states which was further supported by the photocatalysis of a test contaminant. Irradiation induced luminescence enhancement (IILE)[19] technique with different excitation intensities has been studied to explore the interaction of the enzyme with surface states and to justify efficacy of the protein capping agent that shield against deep-UV induced surface damage of the NP surface. In this respect, more biomolecules irrespective of CHT are also promising that may give rise to a new class of multifunctional BNCs with possible biological applications. For example, Lipase L1 enzyme contains an unusual extra domain, making a tight intramolecular interaction with the main catalytic domain through a Zn^{2+}-binding coordination which may offer more novel ZnS BNCs using lipase as a potential host matrix.[20]

2. EXPERIMENTAL SECTION

2.1. Materials. Analytical grade zinc acetate dihydrate, $(CH_3COO)_2Zn\cdot 2H_2O$, manganese acetate tetrahydrate, $(CH_3COO)_2Mn\cdot 4H_2O$, sodium borohydrate, $NaBH_4$, Cystine, α-Chymotrypsin, CHT (MW = 25 kDa), Ala-Ala-Phe-7-amido-4-methyl-coumarin (AAF-AMC), sodium sulphide, Na_2S are from Sigma-Aldrich with highest commercially available purity were used as received. Distilled water from Millipore system was used for preparing all the aqueous solutions.

2.2. Synthesis of NPs. The ZnS:Mn NPs were prepared following a general procedure modified from the reported literature where it was proposed that the growth of nanostructures with different morphologies, sizes, compositions, and microstructures was mainly controlled by the temperature and time duration of the reaction process.[21−30] Briefly, 50 mL each of 0.2 M L-Cys and 20 μM CHT were taken into two different three-necked flasks and 200 μM $NaBH_4$ was added in argon atmosphere with continuous stirring for 45 min. In the next step, 5 mL aqueous solution of 0.1 M zinc acetate was aliquoted into a three-necked round-bottom flask. The mixed solution was adjusted to pH 11.0 by addition of 2 M NaOH and was stirred for 30 min at room temperature and argon atmosphere. Subsequently, 1.5 mL of 0.01 M manganese acetate was added into the above mixture and stirred for 20 min. Five milliliters of 0.1 M deoxygenated Na_2S was then injected into the solution quickly. The mixture was stirred for another 30 min, and then the solution was incubated at 50 °C under air for 2 h to synthesize Cys and enzyme (CHT)-capped ZnS:Mn NPs. Finally, the colloidal NPs were dialyzed against pure water for 4 and 24 h for Cys-Zns:Mn and CHT-ZnS:Mn, respectively, at 4 °C. In this respect, long-term dialysis is the usual practice for protein-capped systems where excess salts may get absorbed into the protein hydrophobic pockets whereas such effects are absent in Cys-capped systems. The Cys-ZnS and CHT-ZnS samples were prepared as above except for the addition of manganese acetate. The overall synthesis process is represented in Scheme 1.

Scheme 1. Synthetic Strategy of Enzyme Mediated Mn-Doped ZnS BNCs

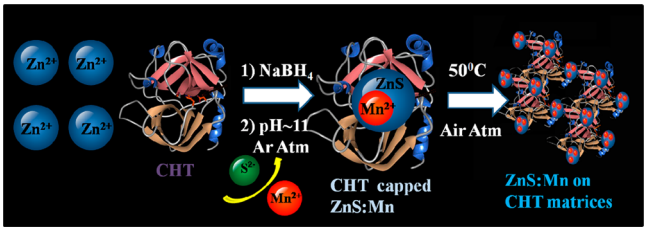

2.3. Characterization. Transmission electron microscopy (TEM) grids were prepared by applying a drop of the colloidal solutions to carbon-coated copper grids. Particle sizes were determined from micrographs recorded at a magnification of 100 000× using an FEI (Technai S-Twin, operating at 200 kV) instrument. X-ray powder diffraction (XRD) patterns were obtained by employing a scanning rate of 0.02° s^{-1} in the 2θ range from 25° to 60° by PANalytical XPERT-PRO diffractometer equipped with Cu Kα radiation (at 40 mA, 40 kV). The zeta potential of the Cys and CHT-capped BNCs in aqueous solvent were measured with a Zetasizer Nano-ZS instrument (Malvern, U.K.). Native and NP-capped enzyme structures has been carried out by circular dichroism (CD) measurements in a JASCO 815 spectro-polarimeter at 20 ± 0.1 °C. The scan speed of the measurements was 50 nm/min, and each spectrum was the average of five scans. The spectral data were acquired over the range of 300−200 nm using a 1 cm path length cuvette and deconvoluted by CDNN 2.1 Simple Spectra software.[31,32] Enzyme activity has been determined by using the kinetic mode of the UV spectrophotometer (monitored at 590 nm wavelength) with enzyme and Ala-Ala-Phe-7-amido-4-methyl-coumarin (AAF-AMC) molar ratio of 1:35. Details of the enzyme activity study are found elsewhere.[33,34] Steady-state absorption and emission spectra were measured with a Shimadzu UV-2450 spectrophotometer and Jobin Yvon Fluoromax-3 fluorimeter, respectively. All the photoluminescence transients were measured using the picosecond-resolved time-correlated single photon counting (TCSPC) technique, a commercially available picosecond diode laser-pumped (LifeSpec-ps) fluorescence spectrophotometer from Edinburgh Instruments, U.K. Picosecond excitation pulses from the picoquant diode laser were used at 375 nm with an instrument response function (IRF) of 60 ps. A microchannel-plate-photomultiplier tube (MCP-PMT, Hammamatsu) was used to detect the photoluminescence from the sample after dispersion through a monochromator. For all transients the polarizer on the emission side was adjusted to be at 55° (Magic angle) with respect to the polarization axis of the excitation beam. Curve fitting of observed fluorescence transients were carried out using a nonlinear least-squares fitting procedure to a function $(X(t) = \int_o^t E(t')\, R(t - t')\, dt')$ composed of the convolution of the IRF $(E(t))$ with a sum of exponentials $(R(t) = A + \sum_{i=1}^{N} B_i e^{-t/\tau_i})$ with pre-exponential factors (B_i), characteristic lifetimes (τ_i) and a background (A). Relative concentration in a multiexponential decay is expressed as, $c_n = (B_n/(\sum_{i=1}^{N} B_i)) \times 100$ The average lifetime (amplitude-weighted) of a multiexponential decay[35] is expressed as, $\tau_{av} = \sum_{i=1}^{N} c_i \tau_i$.

3. RESULTS AND DISCUSSIONS

3.1. Characterization of NPs in the BNCs. Figure 1 shows a set of transmission electron microscopic (TEM) images of CHT and Cys-capped, with/without Mn-doped ZnS NPs. It has to be noted that the shape of the NPs in the protein matrix is relatively quasi-spherical compared to that of the Cys-capped NPs. The observation could be consistent with the fact that the NPs in the protein matrix are associated with a number of sulfur containing Cys residues from various locations of a protein which essentially direct the shape of the NPs to be quasi-spherical. On the other hand, plenty of free Cys residues in the solution for the Cys-capped NPs lead to uniform growth of the NPs and make the shape to be spherical. The corresponding high resolution TEM (HRTEM) images (right insets, Figure 1a−d) clearly demonstrate lattice fringes with an observed d-spacing of ∼0.31 nm and ∼0.23 nm for CHT and Cys-capped NPs, respectively, which are in good agreement with the high-crystallinity in the materials with zinc-blende structures.[10,36] The particle sizes are estimated by fitting our experimental TEM data on 100 particles which provides the average diameter of 3 and 2.7 nm for CHT and Cys-capped NPs (left insets, Figure 1b, d), respectively. It is noticeable that CHT-capped NPs are fairly monodispersed in the protein matrix while for Cys-Zns:Mn, some of the particles are agglomerated up to 10 nm. Owing to the amino group capping on the surface, all the BNCs can be steadily dispersed in water

dx.doi.org/10.1021/ic301083g | Inorg. Chem. 2012, 51, 10203−10210

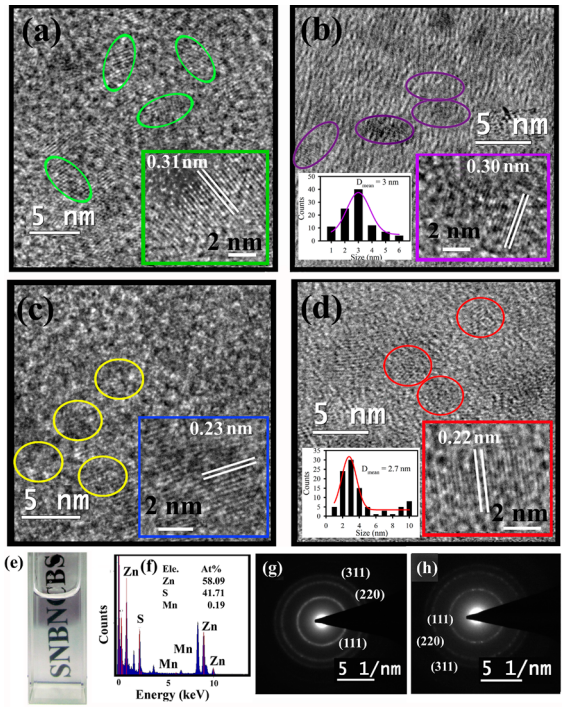

Figure 1. TEM and HRTEM images (inset) of (a) CHT-ZnS, (b) CHT-ZnS:Mn, (c) Cys-ZnS, (d) Cys-ZnS:Mn NPs. Inset left of panels (b) and (d) represent the size distribution analysis of CHT-ZnS NPs and Cys-ZnS:Mn NPs, respectively. (e) Optically transparent solution of CHT-ZnS:Mn BNCs under daylight. (f) EDAX analysis and atomic percentages elements, (g) and (h) SAED analysis of CHT-ZnS and CHT-ZnS:Mn BNCs, respectively.

to form an optically transparent solution (Figure 1e). Further confirmation of the composition and the crystal structure of as-prepared NPs are also evident from Energy-dispersive X-ray spectroscopy (EDAX) and selected area electron diffraction (SAED) analysis. EDAX analysis (Figure 1f) of the CHT-capped NPs reveals the incorporation of Mn with atomic contribution of 0.2% as dopant. A detailed analysis of SAED pattern of CHT-capped (Figure 1g,h) and Cys-capped NPs (see Supporting Information, Figure S1) exhibits a cubic structure with distinct rings consistent with (311), (220), and (111) planes.[28,37]

A typical XRD pattern for CHT-ZnS and CHT-ZnS:Mn BNCs is shown in Figure 2. The spectrum shows three diffraction peaks at 2θ values of 28.9°, 32.4°, 47.5°, and 56.5° which appear because of reflection from the (111), (200), (220), and (311) planes of the cubic phase of ZnS, respectively. The obtained peak positions correspond to zinc blended type patterns for all the samples.[26,38] Particle sizes from XRD patterns were estimated using Scherrer's equation $D = (0.9\lambda)/\beta \cos\theta$, where D is the mean grain size, λ is the X-ray wavelength (for CuKα radiation, λ = 0.15406 nm), θ is the diffraction angle (in radian), and β is full width at half-maximum. The grain size of CHT-ZnS and CHT-ZnS:Mn BNCs, as calculated by using Scherrer's equation, is in range of ~20.7 nm. It must be emphasized that the distinction between XRD and TEM data may be due to the presence of more than one crystallite in single grain, and the size determined by diffraction methods corresponds to the magnitude of the coherent crystal regions, that is, to regions where the periodic arrangement of the atoms is perfect and continuous. Furthermore, there may be some extent of agglomeration among the particles during the preparation of the

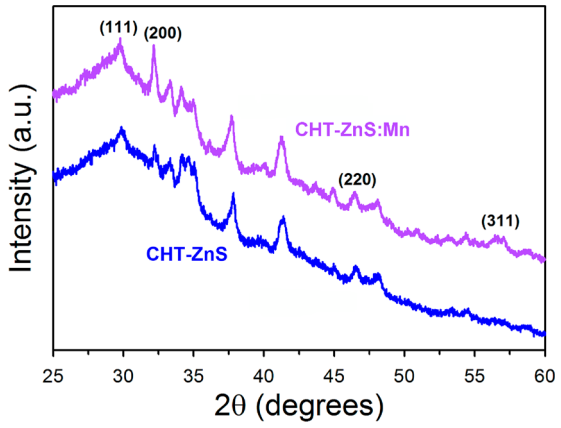

Figure 2. XRD pattern of CHT-ZnS and CHT-ZnS:Mn BNCs at room temperature.

samples for XRD measurement where the aqueous solution of the BNCs was lyophilized using Heto Power Dry LL1500 freeze-dryer instrument and the powder form was used for XRD study. Therefore, the size obtained by diffraction cannot always be simply compared to the sizes determined by other techniques.

Many NPs in solution bear an electrostatic charge on their surface that hampers the interparticle interaction/aggregation by electrostatic repulsion. This surface charge of NPs is very important for defining the composition of the produced BNCs and also has an impact on their subsequent biodistribution. Generally, the zeta potential (ζ potential) gives information on the surface charge of the NPs and can be used to detect protein binding to the NP surface as this will change the overall surface charge.[17,39] The increase in electrophoretic mobility from −1.35 (Cys-ZnS:Mn) to −2.93 μm.cm/V.s (CHT-ZnS:Mn) confirmed the charging of the colloid surface through protein attachment. A change in the ζ potential of the particles was observed from approximately −17.2 mV for a Cys-ZnS:Mn surface[40] to −37.3 mV, as expected for CHT-stabilized particles.[41]

3.2. Protein Structure and Enzymatic Activity in the BNCs. Figure 3a shows circular dichroism (CD) spectra of the BNCs in aqueous solution, and it has been compared with the spectrum of free CHT as a reference. From the CD spectra, a significant perturbation of the secondary structure of the NP-associated enzyme CHT is clearly noticeable. A careful analysis of the secondary structure (inset) of CHT upon attachment with NPs illustrates the variation in the content of helix and antiparallel β-sheet. The consequences of the structural perturbation on the enzymatic activity of CHT in the BNCs are also evident from Figure 3b. In comparison to free enzymes, the NP-associated enzymes in BNCs show a significant retardation of the rate of formation of product (7-amido-4-methyl-coumarin) from the substrate (AAF-AMC). We have estimated that the activity of the BNCs to be 3.8 units/mg, which is significantly retarded compared to that of the free enzyme (21.3 units/mg) in aqueous solutions.[42] It is to be noted that the possibility of CHT to remain as a free enzyme is negligibly small by considering 1:1 binding between CHT and NP since the concentration of the NP (~ 25 μM) is comparable to the initial enzyme concentration (20 μM) in the medium.

3.3. Optical Spectroscopy and Ultrafast Dynamics of the BNCs. We show the optical characterization of these BNC samples in terms of UV−visible absorption spectra and fluorescence spectra in Figure 4. The UV−vis absorption spectra (Figure 4a, b) show a distinct absorption-edge at 320 nm for all

dx.doi.org/10.1021/ic301083g | Inorg. Chem. 2012, 51, 10203−10210

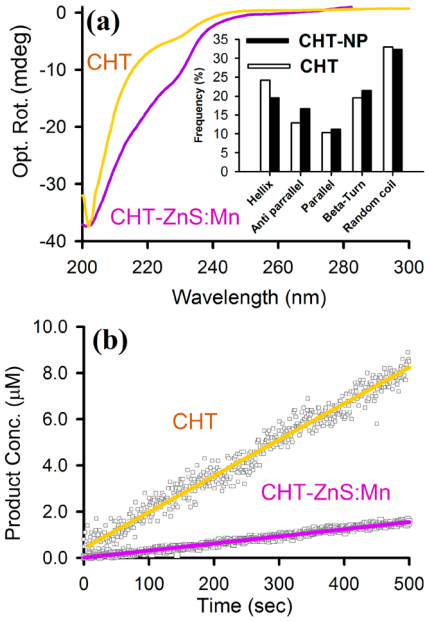

Figure 3. (a) Circular dichroism (CD) spectra of native CHT and CHT-ZnS:Mn BNCs. Inset showing the deconvolution of CD spectra for different fragments of enzyme with native CHT, (b) the enzyme activity kinetics at 270 nm of native CHT and CHT-ZnS:Mn.

the Cys and CHT-capped samples. Effective mass approximation[43] for the estimation of particle size from the shoulder of the absorption spectra of all samples at 320 nm reveals relatively larger particle size (5.3 nm) compared to that observed in the TEM image. The discrepancy could be due to the quasi-broad particle size distribution as evidenced in the TEM studies. It has also been shown earlier that UV−vis spectroscopy essentially reveals larger particles of samples containing multiple particle size distribution.[44,45]

The room temperature PL spectra (Figure 4a, b) of doped and undoped ZnS NPs have been recorded at an excitation wavelength of 300 nm (4.13 eV). As shown in Figure 4b, Cys-capped undoped ZnS NPs show one broad emission band centered at ∼420 nm, which is attributed to defect-state recombinations, possibly at the surface. Since, an excess of the cations have been used in the synthesis procedure, we expect sulfur vacancies at the surface giving rise to Zn dangling bonds that form shallow donor levels. Thus, the recombination is mainly between these shallow donor levels and the valence band. Becker et al. reported that S^{2-} vacancies even in bulk ZnS lead to emission at 428 nm.[46] Upon Mn incorporation in nanocrystal samples, blue ZnS emission is quenched whereas an orange emission band develops at ∼590 nm (Figure 4b), corresponding to the spin forbidden $^4T_1$-$^6A_1$ Mn d-d transition in a tetrahedral site.[47−49] The insets of Figure 4a, b show PL photographs from the undoped (blue) and doped (orange) solutions upon 300 nm excitation. In the CHT-capped BNCs, NP associated proteins show a strong emission band centered at 367 nm (Figure 4a) which possibly augments ZnS PL band at 420 nm.[50] In the picosecond-resolved emission study (Figure 4c), the excited state population of charge carriers in Cys-ZnS:Mn NPs are monitored at 420 nm followed by excitation at 300 nm. It is to be noted that Cys-ZnS and Cys-ZnS:Mn sample solutions show almost the same decay pattern (time constants) when both the decays are monitored at 420 nm. This phenomenon reveals that the ZnS PL quenching upon Mn-doping is either static in nature or may be too fast to be resolved in our TCSPC instrument with

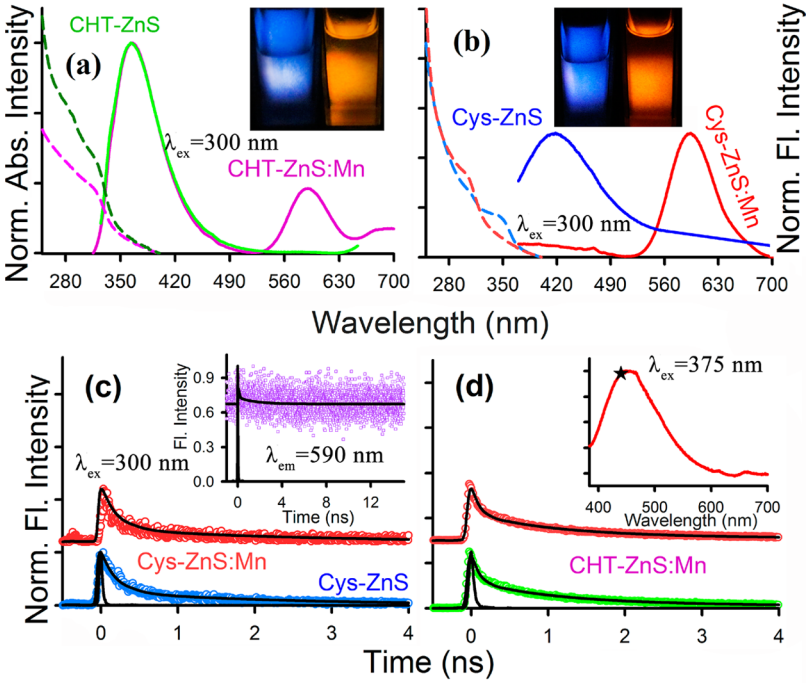

Figure 4. (a) Optical absorption and steady-state emission spectra of (a) CHT-ZnS and CHT-ZnS:Mn BNCs and (b) Cys-ZnS, Cys-ZnS:Mn NPs, respectively. Inset of (a) and (b) shows PL photos of the corresponding solutions upon 300 nm excitation. (c) The picosecond-resolved fluorescence transients of Cys-ZnS and Cys-ZnS:Mn NPs (excitation at 300 nm) collected at 420 nm and inset shows fluorescence transient of Cys-ZnS:Mn NPs collected at 590 nm. (d) The picosecond-resolved fluorescence transients of CHT-ZnS:Mn NPs (excitation at 375 nm) collected at 460 nm (green) (to avoid Raman scattering) and 590 nm (red). Inset shows PL spectra upon 375 nm excitation. A ★ (star) sign represents the appearance of Raman scattering upon 375 nm excitation.

dx.doi.org/10.1021/ic301083g | Inorg. Chem. 2012, 51, 10203−10210

IRF of 60 ps. The inset of Figure 4c shows the time-resolved PL decay of Cys-ZnS:Mn NPs monitored at 590 nm. The PL transient is not completed in our experimental time window revealing higher values of time constants which are reported to be 1−2 ms in previous studies.[7,12] Such a long lifetime makes the luminescence from the NPs readily distinguishable from the background luminescence from ZnS, which has a very short lifetime. On the other hand, in the cases of CHT-ZnS and CHT-ZnS:Mn BNCs, the strong emission from the protein essentially masks the ZnS emission and show characteristic decay of the intrinsic tryptophan residues of the protein in the picosecond-resolved transients at 420 nm (data are not shown). However, it is to be noted that CHT-ZnS:Mn samples show almost same decay pattern of Cys-ZnS:Mn when detected at 590 nm (see Suppurting Information, Figure S2) and as a consequence, these advantages make them ideal candidates as fluorescence labeling agents, especially in biology.[45]

Upon below band-edge excitation (with 375 nm, i.e., 3.3 eV), no Mn emission peak is noticeable in the doped NPs (Figure 4d, inset). The picosecond-resolved fluorescence decays (excitation at 375 nm) monitored at 460 (to avoid Raman scattering at 428 nm) and 590 nm are shown in Figure 4d which exhibits similar time constants of ZnS. The observation suggests that the below-band gap excitation is not sufficient to excite the doped material (Mn) via energy transfer from the host's conduction band to the Mn state.[45] Considering that the excitation process generates an electron−hole pair across the band gap (3.9 eV) of the ZnS nanocrystal host, the present results make it obvious that there is a more efficient excitonic energy transfer from the host to the doped Mn site compared to that of the defect states in these materials; revealing a strong coupling between the Mn d levels and the host states.[51] The energy transfer is unlikely to occur directly from the semiconductor trap (defect) states to the low-lying Mn d-states. This observation demonstrates that the trap states are not in a direct coupling with the Mn d-states and Mn-doping do not affect the trap state lifetimes of the excited state electrons at the host ZnS surface. Details of the spectroscopic parameters and the fitting parameters of the PL decays are tabulated in Table 1.

Table 1. Picosecond-Resolved Luminescence Transients of Cys/CHT-Capped ZnS NPs with/without Mn-Doping[a]

samples	excitation wavelength (nm)	detection wavelength (nm)	τ_1 (ns)	τ_2 (ns)	τ_{avg} (ns)
Cys-ZnS	300	420	0.20 (79%)	2.34 (21%)	0.65
Cys-ZnS:Mn	300	420	0.50 (88%)	3.49 (12%)	0.86
Cys-ZnS:Mn	300	590	4.5 (69%)	42.0 (31%)	16.1
CHT-ZnS:Mn	375	460	0.08 (92%)	2.89 (8%)	0.31
CHT-ZnS:Mn	375	590	0.13 (90%)	3.21 (10%)	0.44

[a]The emissions from ZnS NPs (probing at 420, 460, and 590 nm) were detected with a 300 and 375 nm laser excitation. Numbers in the parentheses indicate relative weightage.

3.4. Photocatalytic Activity of the BNCs. To investigate the efficacy of the host protein matrix in promoting photogenerated charges from ZnS NP to a surface adsorbed molecule, we have performed photocatalysis of an organic dye methylene blue (MB, purchased from Carlo Erba). Bulk ZnS semiconductor with a large band gap (3.6 eV) produces electron−hole pairs under UV light that initiates the formation of surface radicals capable of oxidizing adsorbed organic and biological pollutants.[52,53] As a photocatalyst, ZnS has been examined for degradation of water pollutants, reduction of toxic heavy metals, and water-splitting for H_2 evolution.[54−56] In this work, photocatalytic activity was quantified by carrying out photoreduction of a test contaminant MB (Figure 5a) which is

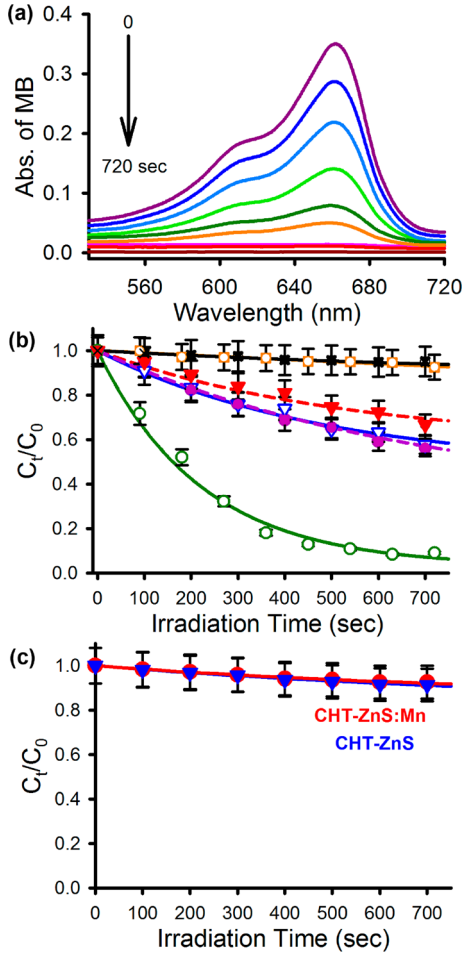

Figure 5. (a) Time dependent UV−vis spectral changes of methylene blue (MB) in the presence of CHT-ZnS BNCs under UV-light irradiation. (b) Plot of relative concentration (C_t/C_0) versus irradiation time for the degradation of MB (monitored at 655 nm) is shown. The degradation is performed in the presence of BNCs: CHT-ZnS (empty circle), CHT-ZnS:Mn (filled circle), Cys-ZnS (empty triangle), Cys-ZnS:Mn (filled triangle), only CHT (empty square), no catalysts (crossed). (c) Plot of C_t/C_0 versus irradiation time in the presence of CHT-ZnS (filled triangle) and CHT-ZnS:Mn (filled circle) upon selective excitation with a 350 nm high-pass filter.

known to be an excellent probe for the study of interfacial electron transfer in colloidal semiconductor systems.[57,58] It is obvious that the higher the charge migration from the surface of the ZnS semiconductor, the faster will be the degradation of the surface-attached MB. Under selective UV radiation, we have recorded the absorption peak of MB (at 655 nm) at 90 s intervals, using SPECTRA SUITE software supplied by Ocean Optics, and plotted it against the time of photoirradiation. The decrease in the absorbance at 655 nm implies the reduction of MB to colorless leuco methylene blue (LMB). Results of MB degradation in the presence and absence of 25 μM ZnS photocatalysts under UV light are shown in Figure 5b, where the relative concentration (C_t/C_0) of MB in solution is plotted with respect to UV irradiation time. The control experiments performed for several hours in the absence of catalysts and/or

dx.doi.org/10.1021/ic301083g | Inorg. Chem. 2012, 51, 10203−10210

without UV irradiation have only resulted in a negligible change in the MB concentration. All the photodegradation curves were found to follow a first-order exponential equation $y = A\exp(-kt) + y_0$, and the kinetic parameters are represented in Table 2. The percentages of total photodegradation (i.e., the value of A in the first-order kinetic equation shown in Table 2) are found to be enhanced in CHT-ZnS compared to Cys-capped NPs. This observation clearly reveals the molecular recognition of MB molecules by the ZnS-attached protein, which can effectively host both ZnS and MB molecules; consequently the electron transfer process is facilitated when electron donor and acceptor molecules come to a close proximity. It is to be noted that CHT contains amino acids with aromatic rings in their side-chains which can act as hydrophobic host sites where the organic dye MB (with aromatic rings) can be incorporated efficiently.[59] It is also revealed that the photocatalytic activity of photocatalyst decreases upon Mn-doping which is consistent with the fact that excited electrons of ZnS can resonantly transfer their energy to the Mn^{2+} state via nonradiative processes. As a consequence, in the presence of Mn, excited electrons are unable to migrate from the ZnS surface to perform the reduction of MB. In contrast, Cys is not composed of hydrophobic aromatic rings in its side chain which can provide efficient binding of MB molecules to facilitate the electron transfer from ZnS to MB. Therefore, the photocatalytic activity itself becomes very poor for Cys-ZnS NPs which decreased further with Mn-doping.

Table 2. Kinetics Parameters[a] for the Photodeterioration of Methylene Blue (MB) in the Absence and Presence of ZnS

samples	k (s^{-1})	total amount of degradation (A %) (in 720 s)	R^2
	Above Band-Edge Excitation		
CHT-ZnS	4.5×10^{-3}	94	0.95
CHT-ZnS:Mn	2.0×10^{-3}	45	0.94
Cys-ZnS	1.9×10^{-3}	41	0.90
Cys-ZnS:Mn	1.4×10^{-3}	32	0.95
CHT	1.1×10^{-3}	8	0.94
no catalyst	9.9×10^{-4}	7	0.88
	Below Band Gap Excitation		
CHT-ZnS	1.1×10^{-3}	10	0.92
CHT-ZnS:Mn	1.0×10^{-3}	9	0.94

[a]Kinetic constants (k), percentages of photoselective degradation (A), and the regression coefficients (R^2).

We have also performed the photocatalysis of MB under selective below-band gap excitation of ZnS NPs to investigate the role of surface trap states in the semiconductor. For this, a 350 nm (3.3 eV) high pass (HP) filter was used to excite ZnS BNCs, which effectively excite electrons to its trap states (below the band gap) rather than exciting electrons to the conduction band of the semiconductor (as evidenced by the PL study). From the photodegradation of MB in the presence of ZnS and ZnS:Mn BNCs with a 350 HP filter, it is clearly shown that no considerable change in the absorbance peak at 655 nm takes place upon below-band gap excitation (shown in Figure 5c). It reveals that the electron transfer is not allowed from ZnS/ZnS:Mn to MB upon direct excitation of electrons to the trap states in BNCs.

3.5. Irradiation Induced Luminescence Enhancement (IILE) Effect of the BNCs. To investigate the efficacy of the protein shell around the BNCs against the UV damage of the encapsulated NPs, we have performed IILE studies under different irradiance doses on both CHT and Cys-capped nanostructures. Earlier, several mechanisms have been proposed to explain the increase in quantum efficiency for UV-irradiated ZnS:Mn NPs.[60,61] More recently, the model[32] involving the migration of electrons fromthe ZnS band to the Mn^{2+} state is found to be more acceptable and further justified by experimental evidence.[62] Being exposed under the UV irradiation, the population of the surface quench centers of the NPs decreases because of either photochemical or photophysical processes; luminescence of Mn^{2+} ions is thus enhanced. The reported studies on the IILE in a polymeric host matrixes and shell capping reveal the minimum damages on NPs' surfaces.[15,62] Our experimental observations of the IILE detection wavelength (at 590 nm)[63] from various Mn-doped samples, as shown in Figures 6a–d, reveal common temporal characteristics. At the beginning, the emission intensity decreases following a plateau region and finally increases monotonically. We have divided the IILE spectra of CHT and Cys-capped NPs into three different zones, short-term degradation (STD),[64] plateau (stable) and IILE, respectively. It is obvious from the figures that the stable zones for the Cys-capped NPs are negligibly small compared to that of the CHT-capped BNCs

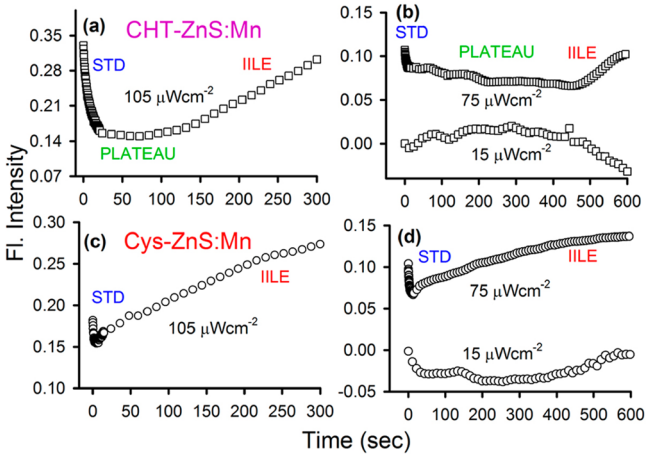

Figure 6. Dose-dependent IILE spectra of (a–b) CHT-ZnS:Mn and (c–d) Cys-ZnS:Mn. The figures clearly demonstrate the individual stable and damage zones of both the systems due to the IILE effect.

Scheme 2. Schematic Representation of a CHT-ZnS:Mn BNC Revealing Its Multifunctional Nature Towards Molecular Recognition, Efficient Photocatalysis, Active Enzyme Catalysis, and Deep-UV Durability

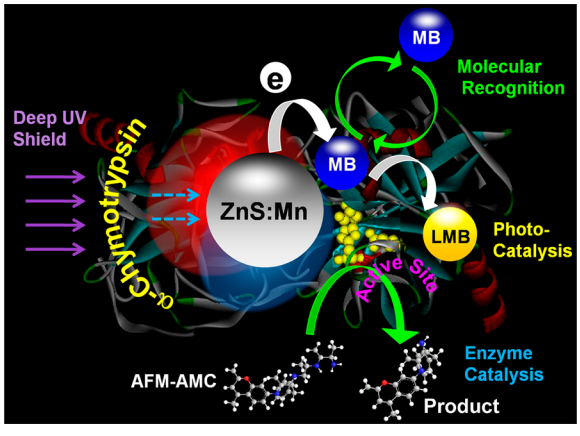

dx.doi.org/10.1021/ic301083g | Inorg. Chem. 2012, 51, 10203–10210

under similar UV exposure. In the first few seconds of UV irradiation, a sudden drop of the initial intensity on a short time scale (assigned as STD zone) was observed, for both Cys and CHT-capped systems, which can be attributed, for the sudden excitation the defect state oxygen in the conduction band act, as a quenching source and equilibrated within few seconds. The indications of surface damage of Cys-capped NPs at lower UV doses (15 μW cm^{-2} dose and 75 μW cm^{-2}) in the STD and IILE processes are still observed (Figure 6d). A negligible damage of the NPs in the BNCs under similar UV exposure (15 μW cm^{-2} and 75 μW cm^{-2} dose) is clearly evident from the Figure 6b. The observation is consistent with the fact that enzyme has relatively more protecting ability against the UV-induced photochemical/photophysical damage on the surface NPs compared to that of the Cysteine amino acid.

4. CONCLUSIONS

In this Article, we show that biomolecules and nanoparticles can be linked to prepare a novel bionanocomposite that is able to recognize and efficiently reduce target organic molecules. A simple, fast, water-soluble, and green phosphine free colloidal synthesis strategy has been developed for the preparation of multifunctional protein (enzyme)-capped ZnS NPs with/without transitional metal-ion doping. While HRTEM and XRD confirm the crystallinity of the BNCs, CD spectroscopy clearly reveals the structural detainment of the host enzyme. The enzymatic activity of the as-prepared BNCs confirms functional intactness of the enzyme to a certain extent. The photocatalytic study by probing an organic dye in the presence of BNCs reveals the molecular recognition of such dyes by the BNCs. The IILE experiments demonstrate the protecting ability of the protein as a capping host against the deep UV damage of the NPs. The overall functionality of the synthesized BNCs is schematically represented in Scheme 2. Our studies may find relevance in the use of water-soluble, stable, enzyme-capped Mn-doped ZnS BNCs for photonic device and bioimaging applications.

■ ASSOCIATED CONTENT

Supporting Information

Investigation of SAED pattern of Cys-capped nanoparticles and the picosecond-resolved fluorescence transients of CHT-ZnS:Mn BNCs. This material is available free of charge via the Internet at http://pubs.acs.org.

■ AUTHOR INFORMATION

Corresponding Author

*E-mail: skpal@bose.res.in.

Author Contributions

†Both authors contributed equally.

Notes

The authors declare no competing financial interest.

■ ACKNOWLEDGMENTS

A.M. thanks CSIR (India) and S.S. thanks UGC (India) for fellowships. We thank DST (India) for the funding (SR/SO/BB-15/2007). We would like to acknowledge Dr. Abhijit Saha, UGC DAE-CSR, India, for measuring the zeta potential of BNCs.

■ REFERENCES

(1) Beaulac, R.; Archer, P. I.; Rijssel, J. V.; Meijerink, A.; Gamelin, D. R. *Nano Lett.* **2008**, *8*, 2949−2953.

(2) Schmidt, T.; Scheibner, M.; Worschech, L.; Forchel, A.; Slobodskyy, T.; Molenkamp, L. W. *J. Appl. Phys.* **2006**, *100*, 123109.

(3) Bryan, J. D.; Gamelin, D. R. *Prog. Inorg. Chem.* **2005**, *54*, 47−126.

(4) Norris, D. J.; Yao, N.; Charnock, F. T.; Kennedy, T. A. *Nano Lett.* **2001**, *1*, 3−7.

(5) Norberg, N. S.; Parks, G. L.; Salley, G. M.; Gamelin, D. R. *J. Am. Chem. Soc.* **2006**, *128*, 13195−13203.

(6) Pradhan, N.; Peng, X. *J. Am. Chem. Soc.* **2007**, *129*, 3339−3347.

(7) Bol, A. A.; Meijerink, A. *Phys. Rev. B* **1998**, *58*, R15997−R16000.

(8) Aboulaich, A.; Geszke, M.; Balan, L.; Ghanbaja, J.; Medjahdi, G.; Schneider, R. *Inorg. Chem.* **2010**, *49*, 10940−10948.

(9) Norberg, N. S.; Dalpian, G. M.; Chelikowsky, J. R.; Gamelin, D. R. *Nano Lett.* **2006**, *6*, 2887−2892.

(10) Deng, Z.; Tong, L.; Flores, M.; Lin, S.; Cheng, J.; Yan, H.; Liu, Y. *J. Am. Chem. Soc.* **2011**, *133*, 5389−5396.

(11) Charinpanitkul, T.; Chanagul, A.; Dutta, J.; Rungsardthong, U.; Tanthapanichakoon, W. *Sci. Tech. Adv. Mater.* **2005**, *6*, 266−271.

(12) Smith, B. A.; Zhang, J. Z.; Joly, A.; Liu, J. *Phys. Rev. B* **2000**, *62*, 2021−2028.

(13) Dickerson, M. B.; Sandhage, K. H.; Naik, R. R. *Chem. Rev.* **2008**, *108*, 4935−4978.

(14) Konishi, M.; Isobe, T.; Senna, M. *J. Lumin.* **2001**, *93*, 1−8.

(15) Gallagher, D.; Heady, W. E.; Racz, J. M.; Bhargava, R. N. *J. Mater. Res.* **1995**, *10*, 870−876.

(16) Mahmoudi, M.; Lynch, I.; Ejtehadi, M. R.; Monopoli, M. P.; Bombelli, F. B.; Laurent, S. *Chem. Rev.* **2011**, *111*, 5610−5637.

(17) Lundqvist, M.; Stigler, J.; Cedervall, T.; Elia, G.; Lynch, I.; Dawson, K. A. *Proc. Natl. Acad. Sci. U.S.A.* **2008**, *105*, 14265−14270.

(18) Murray, C. B.; Norris, D. J.; Bawendi, M. G. *J. Am. Chem. Soc.* **1993**, *115*, 8706−8715.

(19) Cruz, A. B.; Shen, Q.; Toyoda, T. *Thin Solid Films* **2006**, *499*, 104−109.

(20) Choi, W. C.; Kim, M. H.; Ro, H. S.; Ryu, S. R.; Oh, T. K.; Lee, J. K. *FEBS Lett.* **2005**, *579*, 3461−3466.

(21) Fang, X.; Zhai, T. Y.; Gautam, U. K.; Li, L.; Wu, L. M.; Bando, Y.; Golberg, D. *Prog. Mater. Sci.* **2011**, *56*, 175−287.

(22) Fang, X.; Wu, L.; Hu, L. *Adv. Mater.* **2011**, *23*, 585−598.

(23) Zhou, W.; Schwartz, D. T.; Baneyx, F. *J. Am. Chem. Soc.* **2010**, *132*, 4731−4738.

(24) Zhou, W.; Baneyx, F. *ACS Nano* **2011**, *5*, 8013−8018.

(25) Zou, W. S.; Sheng, D.; Ge, X.; Qiao, J. Q.; Lian, H. Z. *Anal. Chem.* **2011**, *83*, 30−37.

(26) Zhuang, J.; Zhang, X.; Wang, G.; Li, D.; W., Y.; Li, T. *J. Mater. Chem.* **2003**, *13*, 1853−1857.

(27) Zhang, W.; Li, Y.; Zhang, H.; Zhou, X.; Zhong, X. *Inorg. Chem.* **2011**, *50*, 10432−10438.

(28) Quan, Z.; Wang, Z.; Yang, P.; Lin, J.; Fang, J. *Inorg. Chem.* **2007**, *46*, 1354−1360.

(29) Fang, X. S.; Ye, C. H.; Zhang, L. D.; Wang, Y. H.; Wu, Y. C. *Adv. Funct. Mater.* **2005**, *15*, 63−68.

(30) Wu, Q.; Cao, H.; Zhang, S.; Zhang, X.; Rabinovich, D. *Inorg. Chem.* **2006**, *45*, 7316−7322.

(31) Hainz, O.; Wegele, H.; Richter, K.; Buchner, J. *J. Biol. Chem.* **2004**, *279*, 23267−23273.

(32) Banerjee, D.; Pal, S. K. *Langmuir* **2008**, *24*, 8163−8168.

(33) Goswami, N.; Makhal, A.; Pal, S. K. *J. Phys. Chem. B* **2010**, *46*, 15236−15243.

(34) Biswas, R.; Pal, S. K. *Chem. Phys. Lett.* **2004**, *387*, 221−226.

(35) Lakowicz, J. R. *Principles of Fluorescence Spectroscopy*, 2nd ed.; Kluwer Academic/ Plenum: New York, 1999.

(36) Lu, X.; Yang, J.; Fu, Y.; Liu, Q.; Qi, B.; Lu, C.; Su, Z. *Nanotechnology* **2010**, *21*, 115702.

(37) Hudlikar, M.; Joglekar, S.; Dhaygude, M.; Kodam, K. *J. Nanopart. Res.* **2012**, *14*, 865.

(38) Maity, R.; Chattopadhyay, K. K. *Nanotechnology* **2004**, *15*, 812−816.

(39) Rezwan, K.; Studart, A. R.; Voros, J.; Gauckler, L. J. *J. Phys. Chem. B* **2005**, *109*, 14469−14474.

(40) Duran, J. D. G.; Guindo, M. C.; Delgado, A. V.; Gonzalez-Caballero, F. *Langmuir* **1995**, *11*, 3648−3655.
(41) Balastre, M.; Persello, J.; Foissy, A.; Argillier, J. F. *J. Colloid Interface Sci.* **1999**, *219*, 155−162.
(42) Narayanan, S. S.; Sinha, S. S.; Pal, S. K. *J. Phys. Chem. C* **2008**, *112*, 12716−12720.
(43) Brus, L. E. *J. Chem. Phys.* **1983**, *79*, 5566.
(44) Dieckmann, Y.; Clfen, H.; Hofmann, H.; Fink, A. P. *Anal. Chem.* **2009**, *81*, 3889−3895.
(45) Wu, P.; Miao, L.; Wang, H.; Shao, X.; Yan, X. *Angew. Chem., Int. Ed.* **2011**, *50*, 8118−8121.
(46) Bacher, G.; Schomig, H.; Scheibner, M.; Forchel, A.; Maksimov, A. A.; Chernenko, A. V.; Dorozhkin, P. S.; Kulakovskii, V. D.; Kennedy, T.; Reinecke, T. L. *Phys. E (Amsterdam, Neth.)* **2005**, *26*, 37−44.
(47) Bhargava, R. N.; Gallagher, D. *Phys. Rev. Lett.* **1994**, *72*, 416−419.
(48) Sooklal, K.; Cullum, B. S.; Angel, S. M.; Murphy, C. J. *J. Phys. Chem.* **1994**, *100*, 4551−4555.
(49) Levy, L.; Feltin, N.; Ingert, D.; Pileni, M. P. *J. Phys. Chem. B* **1997**, *101*, 9153−9160.
(50) Kim, M. R.; Chung, J. H.; Jang, D. *Phys. Chem. Chem. Phys.* **2009**, *11*, 1003−1006.
(51) Tanaka, M. *J. Lumin.* **2002**, *100*, 163−173.
(52) Fujiwara, H.; Hosokawa, H.; Murakoshi, K.; Wada, Y.; Yanagida, S. *Langmuir* **1998**, *14*, 5154−5159.
(53) Xia, B.; Lenggoro, I. W.; Okuyama, K. *Chem. Mater.* **2002**, *14*, 4969−4974.
(54) Yin, H.; Wada, Y.; Kitamura, T.; Yanagida, S. *Environ. Sci. Technol.* **2001**, *35*, 227−231.
(55) Kudo, A.; Sekizawa, M. *Chem. Commun.* **2000**, 1371−1372.
(56) Kudo, A.; Sekizawa, M. *Catal. Lett.* **1999**, *58*, 241−243.
(57) Sarkar, S.; Makhal, A.; Bora, T.; Baruah, S.; Dutta, J.; Pal, S. K. *Phys. Chem. Chem. Phys.* **2011**, *13*, 12488−12496.
(58) Baruah, S.; Sinha, S. S.; Ghosh, B.; Pal, S. K.; Raychaudhuri, A. K.; Dutta, J. *J. Appl. Phys.* **2009**, *105*, 074308.
(59) Hachisako, H.; Yamazaki, T.; Ihara, H.; Hirayama, C.; Yamada, K. *J. Chem. Soc., Perkin Trans. 2* **1994**, 1671−1680.
(60) Yu, I.; Isobe, T.; Senna, M. *J. Phys. Chem. Solids* **1996**, *57*, 373−379.
(61) Jin, C.; Yu, J.; Sun, L.; Dou, K.; Hou, S.; Zhao, J.; Chen, Y.; Huang, S. *J. Lumin.* **1996**, *66−67*, 315−318.
(62) Cao, L.; Zhang, J.; Ren, S.; Huang, S. *Appl. Phys. Lett.* **2002**, *80*, 4300.
(63) Yu, J.; Liu, H.; Wang, Y.; Fernandez, F. E.; Jia, W. *Opt. Lett.* **1997**, *22*, 913−915.
(64) Jeong, H.; Zou, D.; Tsutsui, T.; Ha, C. *Thin Solid Films* **2000**, *363*, 279−281.